INSTITUTE OF PHYSICS PUBLISHING JOURNAL OF MICROMECHANICS AND MICROENGINEERING
J. Micromech. Microeng. **13** (2003) 873–884 PII: S0960-1317(03)59596-1

A phenomenological lubrication model for the entire Knudsen regime

P Bahukudumbi and Ali Beskok

Mechanical Engineering Department, Texas A&M University, TAMU 3123, College Station, TX 77843, USA

E-mail: Abeskok@mengr.tamu.edu

Received 14 February 2003, in final form 7 May 2003
Published 14 August 2003
Online at stacks.iop.org/JMM/13/873

Abstract
Rarefied gas flows in thin film slider bearings are studied in a wide range of Knudsen numbers (Kn) at low Mach number (Ma) with the objective of developing simple physics-based semi-analytical models. A recently developed modified slip boundary condition for steady plane Couette flows and a generalized high-order velocity slip boundary condition, developed and validated earlier for pressure-driven flows, are used to derive a modified slip-corrected Reynolds lubrication equation in the entire Knudsen regime. In particular, we present results of velocity profiles, pressure distribution and load capacity for various slider-bearing configurations. In addition, we outline a method to accurately predict the drag force induced by air resistance to the track-access-motion of the sliders. The new model is validated by comparisons with numerical solutions of the generalized lubrication equation based on the two-dimensional linearized Boltzmann equation and direct simulation Monte Carlo (DSMC) results available in the literature. The model predicts the velocity profiles, pressure distribution, load capacity and skin friction with good accuracy for a wide range of Knudsen numbers for low subsonic compressible flows.

Nomenclature

b	width of lubrication region
C_1	first-order slip coefficients
C_m	generalized slip coefficient
d_{vhs}	variable hard-sphere molecule diameter
D	inverse Knudsen number, $\sqrt{\pi}/(2Kn)$
h	plate separation
h_o	minimum lubrication thickness
H	non-dimensional film thickness, h/h_o
k	modified Knudsen number, $(\sqrt{\pi}/2)Kn$
Kn	Knudsen number, $\lambda/h = Kn_o/(PH)$
Kn_o	outlet Knudsen number
L	length of lubrication region
Ma	Mach number
$\dot{M}_{\text{P}}$, $\dot{M}_{\text{C}}$	Poiseuille and Couette mass flow rates
P_a	atmospheric pressure
p	pressure, ρRT
P	non-dimensional pressure, p/P_a
Q_{cont}	continuum Poiseuille flowrate coefficient
Q_{P}	Poiseuille flowrate coefficient
$\overline{Q}_{\text{P}}$	normalized flowrate coefficient, $Q_{\text{P}}/Q_{\text{cont}}$
R	specific gas constant
T	temperature
T_o	reference temperature
U_0	lateral wall speed
u, v	flow speeds
X, Y	non-dimensional coordinate, x/L, y/h
x, y	stream-wise and cross-flow directions
α	rarefaction correction parameter
Λ	bearing number, $6\mu U_0 L/\left(P_a h_o^2\right)$
λ	mean free path, $\left(\sqrt{2}\pi n d_{\text{vhs}}^2\right)^{-1}$
μ_o	dynamic viscosity, $(2RT_w/\pi)^{1/2}\rho_o\lambda$
μ_e	effective viscosity
ν	kinematic viscosity
π_{xy}	shear stress, normalized with free molecular value
θ	angle of inclination of the slider bearing
ρ	density
σ_v	tangential momentum accommodation coefficient
τ_{xy}	shear stress

Subscripts

c	Couette
cont	continuum
o	reference
∞	free molecular

1. Introduction

Shear- and pressure-driven gas flows are encountered in several MEMS applications like micro-motors, micro-accelerometers, comb mechanisms and computer hard drives. Magnetic disk storage devices used in most computers today utilize a flying head slider suspended nanometers above the rotating recording surface to support the read/write head. A thin gas-lubricated film formed between the slider and the rotating disk is used to maintain the spacing between them. In order to achieve higher storage densities, the head is required to levitate progressively closer to the spinning platter. A fundamental problem, arises when the magnetic spacing in the slider bearing (h) becomes comparable to the gas mean free path (λ). The ratio of these two length scales is known as the Knudsen number ($Kn = \lambda/h$), where finite values of Kn shows onset of rarefaction effects. Based on the Knudsen number, we classify gas flows as continuum ($Kn < 0.01$), slip ($0.01 < Kn < 0.1$), transition ($0.1 < Kn < 10$) and free molecular ($Kn > 10$) flow [1]. Current IBM disk drives with areal density of the order of 12 Gbit in^{-2} have flying heights as low as 15 nm. An extrapolated physical spacing trend line indicates that for ultra-high density recording systems (100 Gbit in^{-2}), a 5–10 nm clearance between the head and floating media is required. Considering that the mean free path for air is about 65 nm at standard conditions, the current hard drives already operate in the transition flow regime, while the next generation drives will push this limit towards the free-molecular flow regime. Therefore, development of lubrication models valid in a wide range of Knudsen regimes is necessary.

Traditionally, the classical Reynolds lubrication equation has been used to model slider bearings. The Reynolds equation is derived starting from the Navier–Stokes equation with the continuum no-slip boundary conditions [2]. However, rarefaction effects are significant for gas flows in close spacings and appropriate corrections to the Reynolds equation are necessary. Burgdorfer [3] derived a modified Reynolds equation valid strictly in the slip flow regime, by including a first-order velocity slip boundary condition in the original Reynolds equation. Similarly, Hsia and Domoto [4] performed a series of experiments for $0.04 < Kn < 2.5$ using different gases in order to change the mean free path, with bearing gaps of $0.075\,\mu\text{m} \leqslant h \leqslant 1.6\,\mu\text{m}$. They also derived a second-order slip boundary condition and compared experimental results with the predictions of the Reynolds equation employing their second-order boundary condition for a Winchester type slider mechanism.

Slider-bearing flows in the transition and free molecular flow regimes have been extensively investigated using the linearized Boltzmann equation and atomistic simulation methods such as DSMC. Gans [5] utilized the BGK linearized Boltzmann equation and derived an approximate lubrication equation using the method of successive approximations. He concluded that the results of the modified Reynolds equation with the first-order slip boundary condition were equivalent to the solution of his approximate lubrication equation. This prompted Fukui and Kaneko [6] to derive a more accurate generalized lubrication equation valid for arbitrary Knudsen numbers using the linearized Boltzmann equation. The generalized lubrication equation is a flowrate-based model and is obtained by semi-numerically calculating the fundamental flows in the lubrication film: Poiseuille, Couette and thermal creep flows. They have shown that the first-order and the second-order (slip-based) Reynolds equations cannot be valid for $Kn \geqslant 1$. Utilization of atomistic simulation methods such as DSMC for the analysis of ultra-thin gas lubrication problems was initiated by Alexander *et al* [7]. For low subsonic slider motion, they found good agreement between their hard-sphere DSMC results and the predictions of the generalized lubrication equation. More recently, Huang and Bogy [8] used the DSMC method to simulate gas flows in a three-dimensional slider bearing with Knudsen numbers as large as 35. Using DSMC, Liu and Ng [9] studied the effects of slider posture (attitude of flying head) and disk speeds on slider-bearing performance. However, the computational complexity and storage requirements associated with the DSMC method or the linearized Boltzmann equation solvers are prohibitive and often inappropriate for the engineering analysis. It is therefore desirable to develop analytical or semi-analytical models, which can accurately describe rarefied gas flow characteristics in close-spaced slider bearings.

In this paper, we develop self-consistent semi-analytical slip models to accurately predict the velocity profiles and lubrication characteristics in ultra-thin gas lubricating films. Earlier efforts [4, 10–12] to derive uniformly valid slip-corrected Reynolds equations using high-order or arbitrary forms of the slip boundary conditions had limited success. These previous studies resulted in accurate predictions of the pressure distribution and integral quantities like the load capacity. However, they were not able to accurately model the velocity distribution in the lubricating film or predict the shear stress. As a result, these models cannot be used to compute the skin friction acting on the runner and slider surfaces separately. (Note that a momentum balance on a control volume will give the total drag force.) Estimation of the skin friction variation is important for robust head-suspension design and to minimize actuator power consumption in hard disk drives. The proposed models can be used to provide a further understanding of the coupled effects of geometry, lateral disk speeds and pressure on performance of the slider bearing, and hence can be utilized for an optimized microfluidic design prior to the fabrication of magnetic hard disk drives and experimental verification. Although the viewpoint of this paper is specific to ultra-thin gas lubrication applications, we emphasize that the model framework can be used to investigate prototype gas flow applications involving combinations of shear and pressure-driven flows. The framework can also be extended to solve a larger class of lubrication problems with varying geometries and surface motion.

This paper is organized as follows: first we describe the fundamental flows in lubricating films, excluding the thermal creep flow. Our modeling approach utilize the Navier–Stokes equations with modified slip boundary conditions and

physical coefficients. We subsequently derive a modified slip-corrected Reynolds-type lubrication equation. The pressure and load capacity characteristics of the slider bearing are then obtained from numerical solutions of the modified Reynolds equation. The proposed model is validated in different rarefaction regions for a wide range of bearing numbers by comparisons with solutions of the generalized molecular lubrication equation and DSMC simulation results. Finally, we outline the procedure to obtain the actual velocity profiles and skin friction in the slider bearing and conclude with a summary and discussion of our results.

2. Models for fundamental flows

In this section, we first briefly review a unified model for the plane Couette flows developed in an earlier work [13]. We then develop a uniformly valid flow model for the Poiseuille flows between parallel plates, following the analysis presented by Beskok and Karniadakis [14] for pressure-driven pipe and duct flows. Special emphasis is placed on accurately modeling the velocity distribution and shear stress in the entire Knudsen range.

2.1. Couette flows

We consider rarefied gas flow between two infinite parallel plates separated by a distance h, and moving with a uniform velocity of $\pm U_0$. Gas flow in the slip flow regime ($0.01 < Kn < 0.1$) is governed by the Navier–Stokes equations and the rarefaction effect is modeled through the partial slip at the wall using Maxwell's velocity slip boundary condition [15] given by

$$u - U_0 = \frac{2-\sigma_v}{\sigma_v} C_1 \lambda \frac{\mathrm{d}u}{\mathrm{d}y} \tag{1}$$

where u is the gas slip velocity, $C_1 = 1.111$ is the first-order slip coefficient due to Ohwada *et al* [16] and σ_v is the tangential accommodation coefficient ($\sigma_v = 1$ for diffuse reflections and $\sigma_v = 0$ for specular reflections). In recent work [13], we demonstrated that the first-order slip model resulted in significant error in the velocity profile in the transitional and free molecular flow regimes. Hence, we developed a unified model for shear-driven gas flows that included analytical expressions for the velocity distribution and shear stress. The velocity model is based on the following modified slip boundary condition, and it accurately predicts the bulk flow velocity distribution for $Kn < 12$ [13]:

$$\begin{aligned} u - U_0 &= \frac{2-\sigma_v}{\sigma_v} C_m \lambda \frac{\mathrm{d}u}{\mathrm{d}y} \\ C_m &= \beta_0 + \beta_1 \tan^{-1}(\beta_2 Kn^{\beta_3}) \end{aligned} \tag{2}$$

where $Kn = \lambda/h$, and $\beta_0 = 1.2977$, $\beta_1 = 0.718\,51$, $\beta_2 = -1.174\,88$, $\beta_3 = 0.586\,42$ are empirical coefficients. The generalized slip coefficient (C_m) can be viewed as a correction term applied to extend the validity of the original Maxwell's first-order slip boundary condition (equation (1)). Note that the modified slip boundary condition converges to the first-order slip model for $Kn < 0.1$. Starting from the Navier–Stokes equations, and assuming steady fully developed incompressible flow, the streamwise momentum equation can be reduced to

$$\frac{\mathrm{d}^2 u}{\mathrm{d}y^2} = 0. \tag{3}$$

Using the modified slip boundary condition given by equation (2), we obtain the following linear velocity distribution (u_c):

$$u_c(y) = \frac{2U_0}{1 + 2\frac{2-\sigma_v}{\sigma_v} C_m Kn} \frac{y}{h}. \tag{4}$$

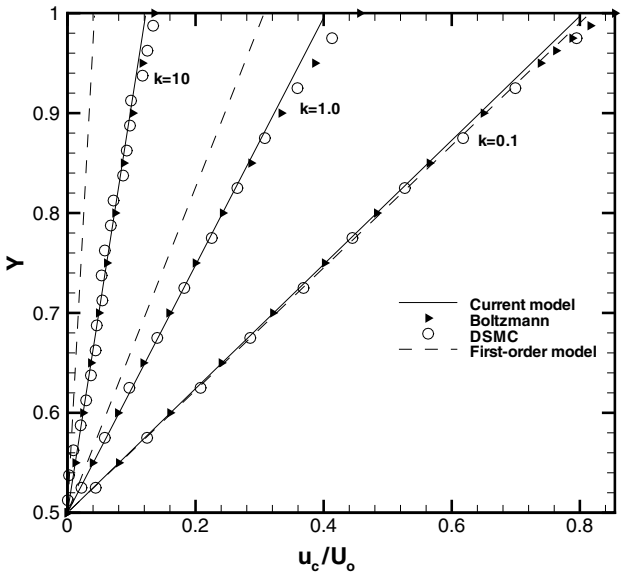

Figure 1. Velocity profiles for linear Couette flow in the upper half of the channel at $k = 0.1$, 1.0 and 10.0. The wall speed corresponds to $Ma = 0.05$.

In figure 1, we present velocity profiles for linear Couette flow in the upper half of the channel at three different Knudsen numbers. The linearized Boltzmann solutions (triangles) and DSMC (circles) agree quite well, and they both predict essentially linear velocity distribution in the bulk flow with significant slip effects for increased Kn. The Knudsen layers are also visible in the figure. The predictions obtained by the new model (solid lines) and the first-order slip model (dashed lines) are also shown in figure 1. Unlike the first-order model, the unified model accurately matches the velocity profile in the bulk flow region for a wide range of the Knudsen numbers. The new slip model is strictly valid for low subsonic flows with the Mach number $Ma \leqslant 0.3$. A more detailed discussion on model validation and limitations can be found in [13].

Shear stress for the Couette flows exhibits two distinct behaviors in the continuum and free molecular flow regimes. Using the classical constitutive laws utilized in the Navier–Stokes equations, shear stress for the plane Couette flow is given by

$$\tau_{xy,\mathrm{cont}} = \mu \frac{\mathrm{d}u}{\mathrm{d}y} = -\mu \frac{2U_0}{h} \tag{5}$$

where the viscosity $\mu = (2RT_w/\pi)^{1/2} \rho_o \lambda$ does not depend on pressure, and the minus sign is due to direction of the shear stress on the fluid. Hydrodynamic approximation of shear stress is proportional to the velocity gradient (angular

deformation rate for 1D flow). This representation is also valid in the slip-flow regime with appropriate velocity slip corrections. In the free molecular flow regime, the shear stress is proportional to the density and relative velocity of the plates, and it is given by [17]

$$\tau_{xy,\infty} = -\rho_o U \sqrt{\frac{2RT_w}{\pi}}. \tag{6}$$

We developed an empirical shear stress model [13] that is accurate in the entire Knudsen regime ($0 < Kn < \infty$) as shown below

$$\pi_{xy} = -\frac{aKn^2 + 2bKn}{aKn^2 + cKn + b} \tag{7}$$

$$a = 0.5296 \qquad b = 0.6029 \qquad c = 1.6276$$

where π_{xy} is the shear stress normalized with the free molecular shear stress. The model uniformly converges to the correct continuum ($Kn \to 0$) and free molecular ($Kn \to \infty$) limits, enabling consistent asymptotic expansions in both the continuum and free molecular limits.

2.2. Poiseuille flows

The Navier–Stokes level constitutive equations along with the appropriate velocity slip boundary conditions can be used to model pressure-driven flows in the slip and early transitional flow regimes. A number of investigators have considered semi-analytical or numerical solutions of the linearized Boltzmann equation to investigate the Poiseuille flow between two parallel plates in the transition and free molecular flow regimes. Cercignani and Daneri [18] obtained accurate numerical solutions of the BGK Boltzmann equation for the Poiseuille flow problem. Other investigators have derived solutions based on the hard-sphere and Maxwellian models for the collision integral [19–21]. In previous work, Beskok and Karniadakis [14] developed unified flow models for pipes and ducts under pressure-driven flow conditions. Using the following generalized high-order velocity slip boundary condition, they developed a physics-based empirical flow model, which predicts the velocity profile, flowrate and pressure distribution in pipes and rectangular ducts in $0 < Kn < \infty$ [14]:

$$u_s - u_w = \frac{2 - \sigma_v}{\sigma_v}\left[\frac{Kn}{1 - b_o Kn}\left(\frac{\partial u}{\partial y}\right)_s\right] \tag{8}$$

where b_o is a generalized slip coefficient [14] and $b_o = -1$ for the Poiseuille flows. Note that equation (8) with $b_o = 0$ corresponds to Maxwell's first-order slip boundary condition.

We consider rarefied gas flow between two infinite stationary parallel plates, separated a distance h. We investigate steady one-dimensional pressure-driven flow induced between the plates subject to the following assumptions:

1. Gas molecules undergo diffuse reflections with the walls.
2. Driving pressure gradient is small. Hence, non-equilibrium effects due to large pressure fluctuations are negligible.
3. Temperature fluctuations and viscous heating effects are negligible.

Further assuming fully developed flow, the streamwise momentum equation reduces to

$$\frac{\mathrm{d}p}{\mathrm{d}x} = \mu \frac{\mathrm{d}^2 u}{\mathrm{d}y^2}. \tag{9}$$

The velocity distribution $u_{\mathrm{P}}(y)$ obtained by integrating equation (9) using the generalized velocity slip boundary condition given by equation (8) is

$$u_{\mathrm{P}} = -\frac{h^2}{2\mu}\frac{\mathrm{d}p}{\mathrm{d}x}\left[\frac{Kn}{1+Kn} + \left(\frac{y}{h}\right) - \left(\frac{y}{h}\right)^2\right]. \tag{10}$$

Although equation (10) acurately predicts the shape of the velocity profile, it cannot predict the correct magnitude of the velocity distribution in the transition and free molecular flow regimes. This is expected as the Navier–Stokes equations are invalid in these regimes. In fact, the dynamic viscosity, which represents diffusion of momentum due to intermolecular collisions must be modified to account for the increased rarefaction effects in the transition and free molecular flow regimes. Beskok and Karniadakis derived the following expression for the generalized diffusion coefficient from first principles [14]:

$$\mu(Kn) = \mu_o \left(\frac{1}{1 + \alpha Kn}\right) \tag{11}$$

where μ_o is the dynamic viscosity of the gas at a specified temperature, α is a rarefaction correction parameter that can be obtained from theory and simulations or experiments, and α depends on the geometry (pipes, ducts and 2D channels), the Knudsen number and the surface accommodation coefficient. The generalized diffusion coefficient is introduced into equation (10) to model the rarefaction effects. The velocity distribution is then obtained as

$$u_{\mathrm{P}} = -\frac{h^2}{2\mu_o}\frac{\mathrm{d}p}{\mathrm{d}x}(1+\alpha Kn)\left[\frac{Kn}{1+Kn} + \left(\frac{y}{h}\right) - \left(\frac{y}{h}\right)^2\right]. \tag{12}$$

We can construct a unified shear stress model for the plane Poiseuille flows using the Navier–Stokes level constitutive equations with modified physical coefficients, such as the generalized diffusion coefficient. Combining equations (10) and (11), we can write the Poiseuille flow shear stress as

$$(\tau_{xy})_{\mathrm{Poiseuille}} = \left(\frac{\mu_o}{1+\alpha Kn}\right)\left(\frac{\mathrm{d}u_p}{\mathrm{d}y}\right)_{y=h}. \tag{13}$$

On simplification the shear stress becomes

$$(\tau_{xy})_{\mathrm{Poiseuille}} = \frac{h}{2}\frac{\mathrm{d}p}{\mathrm{d}x} \tag{14}$$

which in essence states that for a fully developed flow, pressure drop along a channel balances the shear stress on the channel surface. It may seem that equation (14) is independent of the Knudsen number. However, the pressure gradient is a strong function of the degree of rarefaction as will be demonstrated later in this paper.

Using the velocity distribution given by equation (12), the following equation for the volumetric flowrate (per channel width) is obtained:

$$\dot{Q}_{\mathrm{P}} = -\frac{h^3}{12\mu_o}\frac{\mathrm{d}p}{\mathrm{d}x}(1+\alpha Kn)\left[1 + \frac{6Kn}{1+Kn}\right]. \tag{15}$$

Normalized with the continuum volumetric flowrate (Q_{cont}):

$$\overline{Q_{\mathrm{P}}} = \frac{\dot{Q}_{\mathrm{P}}}{Q_{\mathrm{cont}}} = \left[1 + \frac{6Kn}{1+Kn}\right](1+\alpha Kn). \tag{16}$$

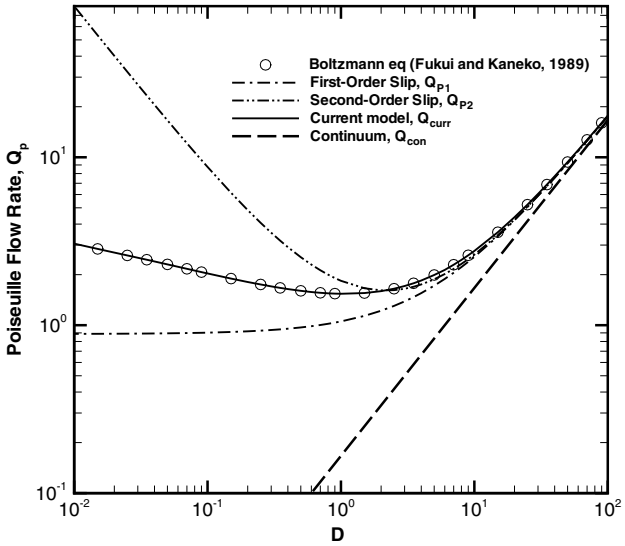

Figure 2. Variation of the Poiseuille flowrate coefficient Q_{P} as a function of the exit inverse Knudsen number. Comparisons of our model with the linearized Boltzmann solution and predictions of other slip models are also shown.

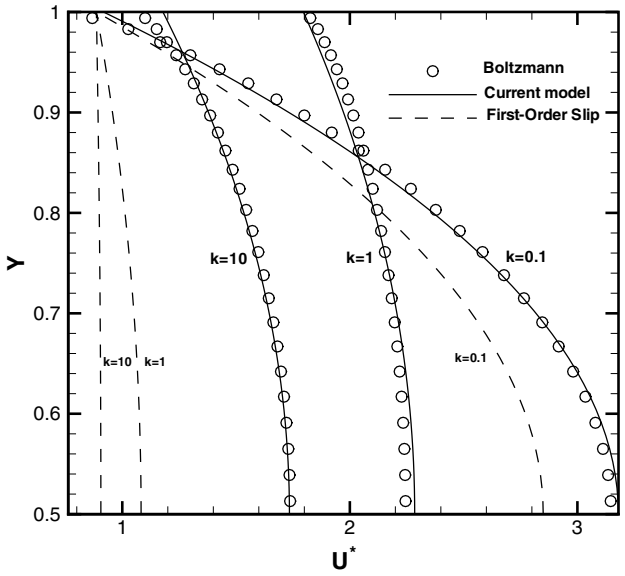

Figure 3. Non-dimensional velocity profiles $(U^* = u_p/(\sqrt{\frac{RT}{2}}\frac{h}{P_a}\frac{\mathrm{d}p}{\mathrm{d}x}))$ of the plane Poiseuille flow in the upper half of the channel for $k = 0.1$, 1.0 and 10.0.

Table 1. Variation of the rarefaction correction parameter (α) with inverse Knudsen number (D) for $\sigma_v = 1$ conditions.

D	$\alpha\ (\sigma_v = 1)$	D	$\alpha\ (\sigma_v = 1)$	D	$\alpha\ (\sigma_v = 1)$
100	0.95113	8	1.6462	0.3	1.7644
90	0.9620	7	1.3696	0.25	1.8014
80	0.9729	6	1.3822	0.2	1.8506
70	0.9836	4	1.4714	0.15	1.9231
60	0.9942	3	1.5061	0.1	2.0406
50	1.0167	2	1.5424	0.09	2.0733
40	1.1562	1	1.5999	0.08	2.1115
35	1.0633	0.9	1.6095	0.07	2.1572
30	1.0870	0.8	1.6206	0.06	2.21103
25	1.1202	0.7	1.6353	0.05	2.2768
20	1.1658	0.6	1.6537	0.04	2.3623
15	1.2235	0.5	1.6786	0.03	2.4758
10	1.3065	0.4	1.7126	0.02	2.6460
9	1.3260	0.35	1.7352	0.01	2.9768

The rarefaction correction parameter, α, was obtained by matching the flowrate model given by equation (16) with the Poiseuille flowrate database obtained via the solution of a two-dimensional Boltzmann equation in [22]. Note that α is a function of both the Knudsen number and surface accommodation coefficients. A database of α values for $\sigma_v = 1$ is given in table 1. Figure 2 compares the Poiseuille flowrate coefficient ($\overline{Q_p}$) calculated using different theories. The proposed model uniformly matches the flowrate in the entire Knudsen number regime and accurately predicts the Knudsen minimum at $Kn = 1.005$. The figure indicates that the second-order slip model is a better approximation than the first-order slip model to the Fukui and Kaneko [22] database in the slip-flow regime. All the models uniformly approach the same limit as the inverse Knudsen number, $D \to \infty$. However, the difference between the various models increases as $D \to 0$.

Solution of linearized Boltzmann equation in a two-dimensional channel results in a logarithmic increase in the flowrate with increased Kn in the free molecular flow limit [22]. This unbounded increase in flowrate is contrary to the three-dimensional behavior, where the duct and pipe flows reach an asymptotic constant flowrate in the free molecular flow limit. This has been documented in the experiments of Gaede [23] and Tison [24] and verified by linearized Boltzmann solutions [20, 25, 26], as well as the DSMC simulations [14]. As a result, the applicability and the accuracy of the Poiseuille flowrate database obtained via the solution of a two-dimensional Boltzmann equation is open to some speculation. Therefore, we expect our model to exhibit some physical limitations in the free molecular flow regime. Our particular choice of using the Fukui and Kaneko database is due to its use as the current industry standard for air bearing design. We must note that our flowrate model can be trained to match any database by suitably changing the value of α, as demonstrated in [14].

In figure 3 we plot the non-dimensional velocity $\left(U^* = u_p\Big/\left(\sqrt{\frac{RT}{2}}\frac{h}{P_a}\frac{\mathrm{d}p}{\mathrm{d}x}\right)\right)$ variation in the upper half of the channel obtained using the proposed model for $k = 0.1, 1.0$ and 10.0, where $k = (\sqrt{\pi}/2)Kn$ is a modified Knudsen number. Note that this choice of non-dimensionalization removes the dependence of velocity distribution on local flow conditions. It also captures both the magnitude and shape of the velocity distribution. We also included the corresponding linearized Boltzmann solutions obtained in [20]. From the linearized Boltzmann solution in figure 3, it is evident that the velocity profiles are approximately parabolic for a large range of Knudsen numbers. This is also consistent with the form of the velocity model derived from the Navier–Stokes equation and given by equation (12). Here we find that equation (12) accurately predicts the shape and the magnitude of the velocity distribution for a wide range of Knudsen numbers. Velocity profile predicted by the first-order slip condition significantly deviates from the linearized Boltzmann solution

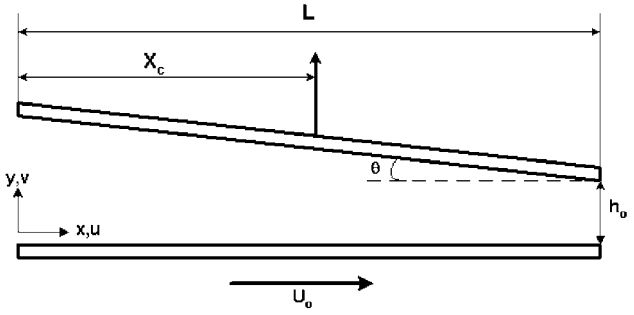

Figure 4. Schematic of the slider-bearing geometry. Streamwise location of the load capacity X_c is also shown.

as the Knudsen number increases. The second-order slip model also becomes invalid beyond $Kn = 0.1$ as shown by Fukui and Kaneko [6].

3. Modified slip-corrected Reynolds equation

Reynolds equation is derived starting from the Navier–Stokes equations. For simplicity, we analyse two plates with a small gap between them. The upper plate is placed with a slight angle, θ (typically less than 1°), with respect to the lower plate, while the latter is moving from left to right with a velocity U_0, as shown in figure 4. We assume that the plate length L is much larger than the magnetic separation h_o and that the plate width b is much greater than h_o. Hence, the flow in the slider bearing is two dimensional.

To obtain the modified slip-corrected Reynolds equation, it is necessary to accurately estimate the massflow rate ($\dot{M}$) in the lubrication film. If temperature variations in the system are neglected, thermal creep effects can be ignored. Then, we can use the linearity of the momentum equation to express the velocity distribution $u(y)$, and hence the mass flowrate $\dot{M}$ as the sum of the Poiseuille and Couette flow components

$$u = u_{\mathrm{P}} + u_{\mathrm{C}} \qquad \dot{M} = \dot{M}_{\mathrm{P}} + \dot{M}_{\mathrm{C}}$$

where u_{P} and u_{C} denote the plane Poiseuille and Couette flow velocities, respectively, while $\dot{M}_{\mathrm{P}}$ and $\dot{M}_{\mathrm{C}}$ represent the massflow rates. Superimposing the velocity distribution of the Poiseuille and Couette flows we obtain

$$u(y) = -\frac{h^2}{2\mu_o}\frac{\mathrm{d}p}{\mathrm{d}x}(1+\alpha Kn)\left[\frac{2-\sigma_v}{\sigma_v}\frac{Kn}{1+Kn} + \left(\frac{y}{h}\right) - \left(\frac{y}{h}\right)^2\right] + \frac{1 + C_m Kn - \frac{y}{h}}{1 + 2C_m Kn}. \tag{17}$$

Using the velocity distribution given above and the local density (ρ), the following equation for the mass flowrate (per channel width) is obtained:

$$\dot{M} = -\frac{\rho h^3}{12\mu_o}\frac{\mathrm{d}p}{\mathrm{d}x}(1+\alpha Kn)\left[\frac{6Kn}{1+Kn} + 1\right] + \frac{1}{2}\rho U_o h. \tag{18}$$

Since the flow is assumed isothermal and in thermodynamic equilibrium, the density can be written as a function of the pressure using the equation of state $\rho = P/RT$. Note that the mass flowrate is a function of the pressure gradient, which is unknown. Furthermore, the left-hand side of equation (18) is a constant, but the right-hand side is a function of x. Taking the gradient of equation (18), we obtain the modified slip-corrected Reynolds equation for one-dimensional steady flow

$$\frac{\partial}{\partial x}\left[(1+\alpha Kn)\left(1+\frac{6Kn}{1+Kn}\right)h^3 p\frac{\mathrm{d}p}{\mathrm{d}x}\right] = 6\mu_o\frac{\partial}{\partial x}(phU_o). \tag{19}$$

Since the spatial variation of channel height (h) is known, the pressure is the only unknown in this equation. The terms in the two parentheses on the left and right of equation (19) are proportional to the mass flowrate per channel width (divided by RT) in the plane Poiseuille and Couette flows, respectively. Note that the flowrate of the linear Couette flow is independent of Kn. The Reynolds equation can be non-dimensionalized by normalizing the pressure using the ambient pressure P_a, and the length-scales in the x- and y-directions with channel length L and h_o, respectively. This results in the non-dimensional modified Reynolds equation

$$\frac{\partial}{\partial X}\left[(1+\alpha Kn)\left(1+\frac{6Kn}{1+Kn}\right)H^3 P\frac{\mathrm{d}P}{\mathrm{d}X}\right] = \Lambda\frac{\partial}{\partial X}(PH). \tag{20}$$

Note that Kn represents the local Knudsen number and is related to the outlet Knudsen number Kn_o as $Kn = Kn_o/(PH)$. Using equation (16) we can rewrite the above equation as

$$\frac{\partial}{\partial X}\left[\overline{Q_p}H^3 P\frac{\mathrm{d}P}{\mathrm{d}X}\right] = \Lambda\frac{\partial}{\partial x}(PH). \tag{21}$$

In fact this is the form of the generalized Reynolds equation derived by Fukui and Kaneko using the linearized Boltzmann equation [6]. However, their approach solely depends of $\overline{Q_p}$ and does not result in analytical expressions for the velocity profile and the shear stress unlike the current model. The continuum Reynolds equation can be obtained from equation (20) by setting $Kn = 0$. The first-order slip Reynolds equation proposed by Burgdorfer [3] can also be deduced from equation (20).

4. Lubrication characteristics

A number of different slider-bearing configurations were analysed using the modified slip-corrected Reynolds equation. The ratio of the inlet to exit plate separation, H_1/H_o, was fixed at two to one, and the effect of Knudsen number and bearing number on lubrication characteristics was examined. The ambient pressure P_a at the inlet and exit boundaries is atmospheric, while the temperature $T_o = 273$ K. In the calculations, we used a second-order finite difference scheme to discretize equation (20). The discretized equations were solved using a direct iteration method, also called Picard's method. We used 400 equally spaced nodal points along the slider length. All calculations were performed to double precision accuracy (16 significant digits). In addition we monitor the residuals of the global conservation of mass. The results presented in this work conserve mass with 99.95% accuracy. The results were also tested for grid independence by increasing the resolution of grid points in the x-direction. In order to validate our model with the existing DSMC results available in the literature [7] and the numerical solutions of

the generalized lubrication equation, we consider the following cases:

(a) $Kn_o = 1.25$, $\Lambda = 61.6$
(b) $Kn_o = 1.25$, $\Lambda = 758$
(c) $Kn_o = 4.167$, $\Lambda = 1264$.

The Reynolds lubrication equation with first-order slip model [3] and the Fukui and Kaneko model [6] were solved numerically using a shooting method that employs a fourth-order Runge–Kutta scheme.

4.1. Pressure distribution

When the gas pressure is ambient, the minimum magnetic spacing of the slider bearing in case (a) is 50 nm. The corresponding DSMC simulation in [7] uses a slider bearing of length $L = 5$ μm and a platter speed $U_0 = 25$ m s^{-1} to obtain a bearing number $\Lambda = 61.6$. This translates to the Mach number $Ma = 0.08$. As the slip-corrected Reynolds equations are valid for only low subsonic flows (typically $Ma < 0.3$), this is an ideal test case to validate the model. Also, unlike the DSMC simulations we consider slider bearings of infinite width. Hence, end effects and side flows cannot be accounted for. In figure 5(*a*), solution of the modified slip-corrected Reynolds equation is compared with predictions of other Reynolds lubrication equations and pressure data obtained from the DSMC simulations of Alexander *et al* [7]. As evident from figure 5 an impressive agreement is found between the proposed model prediction, particle-based simulation results and numerical solutions of the generalized lubrication equation. However, the pressure profile predicted by the first-order slip model exhibits significant deviations from the DSMC data and Fukui and Kaneko's model as expected. The second-order slip model also results in considerable errors in the pressure profile as shown in [9].

Next, we consider a slider bearing with an identical geometric configuration as in case (a). Also, we retain the same value of Knudsen number $Kn = 1.25$, but increase the bearing number to $\Lambda = 758$. The DSMC simulations [7] use very high platter speeds corresponding to the Mach number $Ma = 1.0$. Surprisingly, the pressure profiles predicted by different models are very similar, as seen in figure 5(*b*). This is because of the relatively high-bearing number used in this case. Bearing number is the ratio of Couette and Poiseuille flow rates, as evident from equation (21). Consequently, for high-bearing numbers the plane Couette flow is the dominant flow in the lubricating film. Under these conditions, we can expect the pressure profiles, predicted by the generalized lubrication equation and the Reynolds equation with first-order slip condition to be nearly similar, because of identical terms representing the Couette flows in both models. In the third case, we consider a highly rarefied gas flow with $Kn_o = 4.167$ and a high $\Lambda = 1264$. Under these conditions, the minimum magnetic spacing $h_o = 15$ nm and the Mach number corresponding to the platter speeds is $Ma = 0.5$. The next generation hard drives with ultra-high storage densities would require slider bearings with a similar configuration as in case (c). Again, the solution of the modified slip-corrected Reynolds equation is in good agreement with the Fukui–Kaneko solution and DSMC data. Pressure profile resulting from the first-order slip correction is in fair agreement

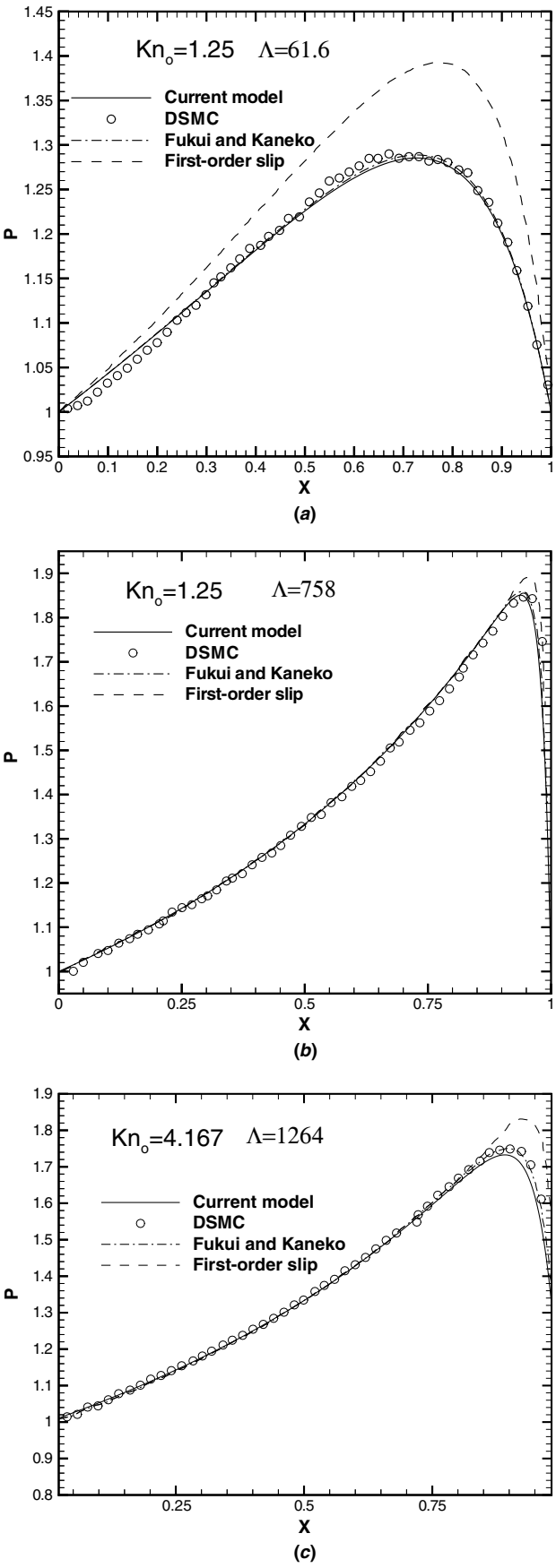

Figure 5. Slider-bearing pressure profiles for different Knudsen number and bearing number combinations.

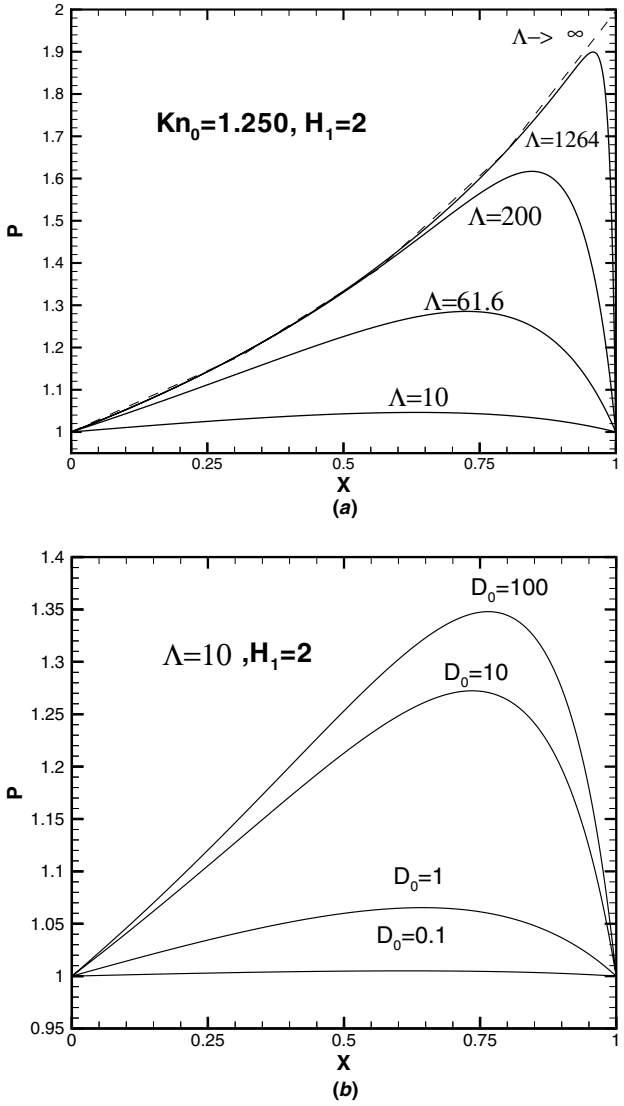

Figure 6. Pressure distribution in the slider bearing for various combinations of the inverse Knudsen number D_o and bearing number Λ, predicted using the modified Reynolds equation.

with the other models despite the large Knudsen number, because of the high-bearing number used. This behavior is better understood by considering the asymptotic solution of the pressure as $\Lambda \to \infty$. Following Gross *et al* [2], we find that the pressure distribution for a slider-bearing uniformly converges to $P \times H =$ constant as $\Lambda \to \infty$.

We can now use the modified Reynolds equation to investigate the lubrication characteristics in different slider-bearing configurations. In figure 6, we present the variation of pressure distribution with the inverse Knudsen number D_o and bearing number Λ. At fixed Kn_o, the pressure distribution increases as the bearing number increases and asymptotes to a solution of a slider bearing with infinite Λ as shown in figure 6(a). In figure 6(b) the bearing number is fixed at $\Lambda = 10$. As a result, the contributions of the Poiseuille flow component is important. The pressure distribution increases as the gas flow in lubricating film approaches continuum conditions from the free molecular flow conditions. The pressure profiles uniformly asymptote to the continuum solution as $D_o \to \infty$.

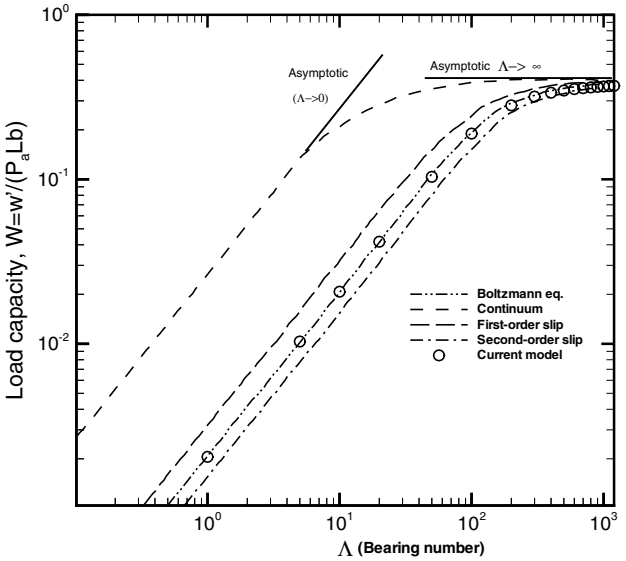

Figure 7. Normalized load carrying capacity as a function of the bearing number at $D_o = 0.5$.

4.2. Load capacity

The load capacity of a slider bearing is representative of the vertical force acting on the flying slider as shown in figure 4. It is an integral quantity obtained directly from the pressure distribution. The read/write functionality of the flying head is a critical function of the magnetic spacing. While its sensitivity exponentially reduces with increasing spacing, a very small flying height can make the read/write head to accidentally scratch or crash into the spinning recording medium. Special emphasis is placed during design to appropriately balance the forces in the vertical and horizontal directions to minimize spacing fluctuations during the operation. Accurate prediction of load capacities is also important for design of the suspension system supporting the read/write head.

The vertical load acting on the upper surface of the slider bearing can be obtained from the load carrying capacity W, defined as

$$W = \frac{w'}{P_a L b} = \frac{1}{P_a L b} \int_0^1 (P - 1) \cos\theta \, \mathrm{d}X. \qquad (22)$$

However, as the angle of inclination is small, typically less than 1°, the surfaces can be assumed to be nearly parallel. Consequently the gas pressure P is constant in the vertical direction and the normalized load capacity becomes

$$W = \frac{1}{P_a L b} \int_0^1 (P - 1) \, \mathrm{d}X. \qquad (23)$$

It is important to note that this definition of load capacity is valid only for bearings with low subsonic slider motion that ensures equilibrium conditions [7]. Figure 7 shows the relationship between the load carrying capacity and the bearing number when the inverse Knudsen number at the outlet is kept constant at $D_o = 0.5$. The load capacity obtained from the modified Reynolds equation accurately matches the Fukui and Kaneko model predictions for a wide range of bearing numbers. Note that all models converge to the same asymptotic constant when $\Lambda \to \infty$. This is also obvious from the behavior of pressure distribution for large bearing numbers discussed in the previous section. However for smaller bearing

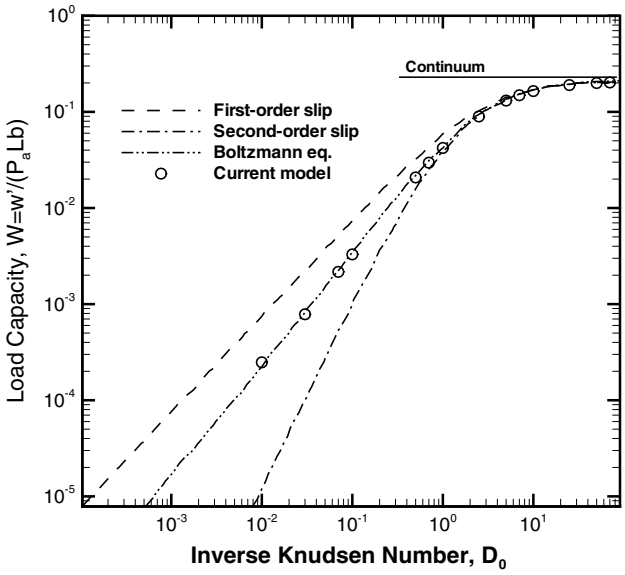

Figure 8. Normalized load carrying capacity as a function of the inverse Knudsen number at $\Lambda = 10$.

numbers, the first-order slip model over-estimates the load capacity while the second-order model under-estimates it. This is expected because the pressure-driven flow component is dominant for lower bearing numbers, and the lower order slip models cannot accurately model the Poiseuille flows in the transition and free molecular flow regimes. In figure 8, we plot the load capacity predicted by various models in different rarefaction regimes. The bearing number is kept constant at $\Lambda = 10$. All models uniformly converge to the well-defined continuum limit as $D_o \to \infty$. The current model uniformly matches the Fukui and Kaneko model for a wide range of Knudsen numbers. The first- and second-order slip models accurately predict the load capacities in the slip flow regime, but systematically deviate from the Fukui and Kaneko model for $D_o < 1$. Pronounced differences between the models are observed for higher Knudsen numbers because of the low bearing number used. It can thus be concluded from figures 7 and 8 that the effect of Knudsen number on load capacity decreases as the bearing number increases.

The streamwise location of the load capacity, X_c, is the focal point of the resultant pressure acting on the slider surface. In [9], Liu and Ng computed X_c for slider bearings with varying angle of inclinations. It is an important design calculation because the pivot point between the head-suspension and the slider should be placed at the streamwise location of the load capacity, X_c. A flexure or a gimbal with low roll or pitch stiffness but high lateral and vertical stiffness acts as the pivot between the head-suspension and the slider. Following Liu and Ng, we define X_c as [9]

$$X_c = \frac{\int_0^1 (P - P_a) X \, \mathrm{d}X}{\int_0^1 (P - P_a) \, \mathrm{d}X}. \tag{24}$$

The numerical pressure data were used to evaluate the integrals in the numerator and the denominator of the above expression. In figure 9, we plot the variation of X_c with the Knudsen and bearing numbers. When the bearing number is held constant at $\Lambda = 10$, the streamwise location of the load capacity moves away from the center of the slider towards the exit as D_o increases. A similar behavior is observed when the inverse Knudsen number is fixed at $D_o = 1.4$ and the bearing number is increased. For the combination of bearing number and Knudsen number cases presented in figure 9, the value of X_c lies between 0.55 and 0.7. Hence, once the configuration of the slider bearing is determined, the position of the pivot point in the suspension system can be obtained from the streamwise location of the load capacity.

4.3. Velocity distribution in the lubricating film

The velocity distribution in the lubricating film, expressed as a composite of the Poiseuille and Couette flows, is given by equation (17). In figures 10 and 11, we plot the velocity distributions at different streamwise locations for two different slider-bearing configurations. The velocity profile predicted using the first-order slip model is also shown using the dashed lines. Note that the velocity is normalized using the bottom plate velocity U_0. Velocity distributions of the current and first-order slip models are based on the local pressure gradients obtained from the respective theories. The corresponding pressure profiles are also included to facilitate comparisons. The velocity distribution in figure 10 corresponds to a slider-bearing configuration with bearing number $\Lambda = 61.6$ and a Knudsen number $Kn = 1.25$. As the bearing number chosen is small, we expect the pressure-driven flow term in the Reynolds equation to become important. The current model has been shown to accurately predict the pressure distribution for a wide range of Knudsen and bearing numbers. Also we can expect equation (17), obtained by the superposition of the uniformly valid Poiseuille and Couette flow models, to accurately model the velocity distribution in the lubricating film. However, significant differences exist in the pressure distribution predicted by the first-order model and the Fukui and Kaneko model. These differences in the pressure distribution result in errors in the velocity distribution. The velocity profiles at different streamwise locations ($X = 0.2, 0.5$ and 0.9) in figure 10 indicates increasing differences between the current model and first-order model as we approach the exit of the slider bearing.

Next, we consider a somewhat extreme scenario. In this case we increase the Knudsen number to $Kn = 4.167$ and choose a very high bearing number $\Lambda = 1264$. As discussed earlier the pressure distribution predicted by the first-order model is in fair agreement, and the current model solution is in good agreement with the Fukui and Kaneko model and the DSMC data. Nevertheless, the velocity profiles at different streamwise locations ($X = 0.2, 0.85$ and 0.95) in figure 11 indicate differences between the current model and the first-order slip model. This is primarily due to the high Knudsen number used in this case, where the first-order slip model cannot accurately predict the velocity profiles in the transition and free molecular flow regimes. The second-order slip boundary conditions also results in similar deviations in the velocity profile [6].

4.4. Drag force

Estimation of drag forces on the floating slider is important especially for the design of the head-suspension system. A shear drag force on the slider surface is induced by the

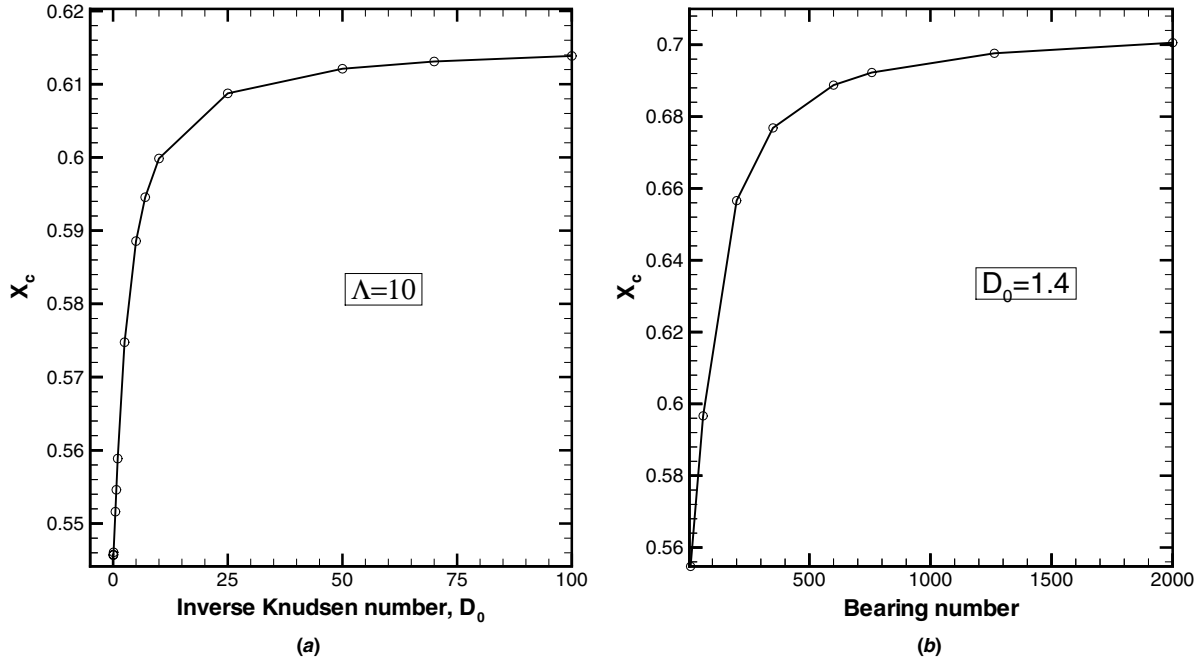

Figure 9. Variation of the streamwise location of load capacity with the inverse Knudsen number D_o and bearing number Λ.

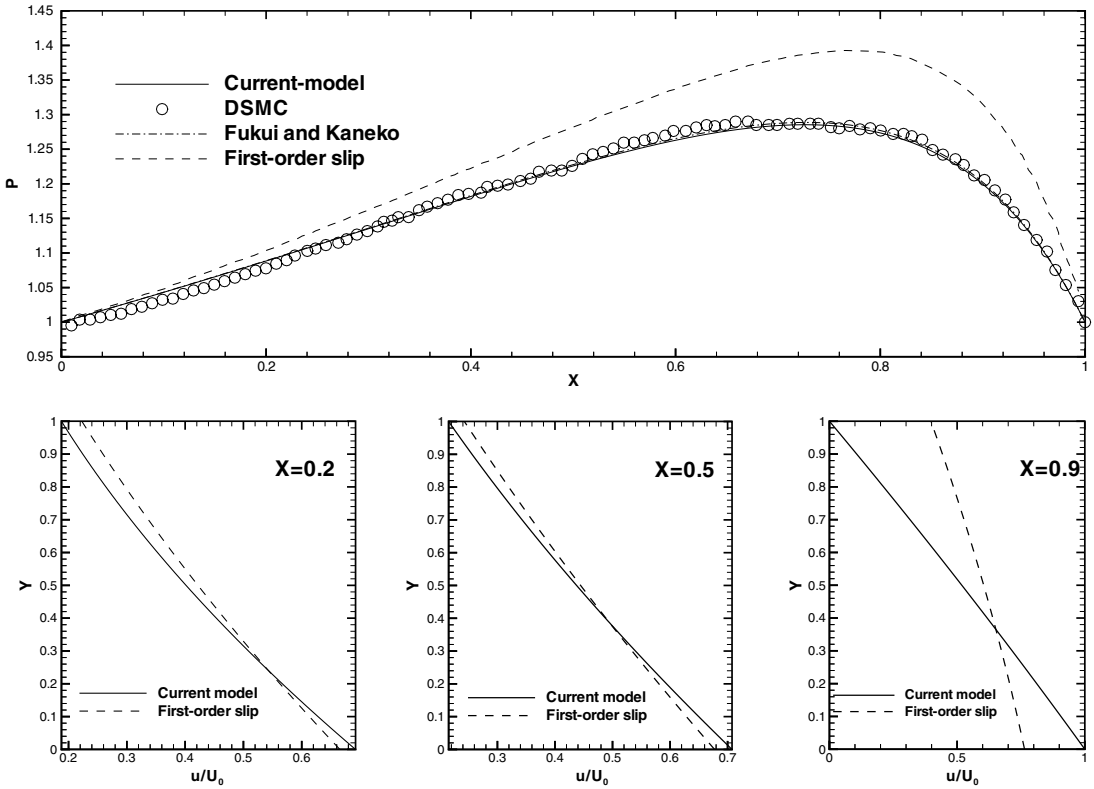

Figure 10. *Top*: pressure distribution for $Kn = 1.25$ and the bearing number $\Lambda = 61.6$. *Bottom*: velocity distribution at various streamwise positions. Predictions based on the current and first-order slip models are shown. The cross-flow direction Y is normalized with the local bearing height $Y = y/h$.

frictional air resistance to the motion of the slider as it sweeps across the magnetic tracks on the recording medium. The pressure acting on the slider surface also contributes to a pressure drag force. Accurate modeling of the drag force is also necessary for prediction of slider dynamics and estimation of the actuator power consumption [27].

The pressure drag force, F_{DP}, acting on the slider surface can be directly obtained from the pressure distribution as

$$F_{\mathrm{DP}} = \int_0^1 P \sin(\theta)\, \mathrm{d}X. \tag{25}$$

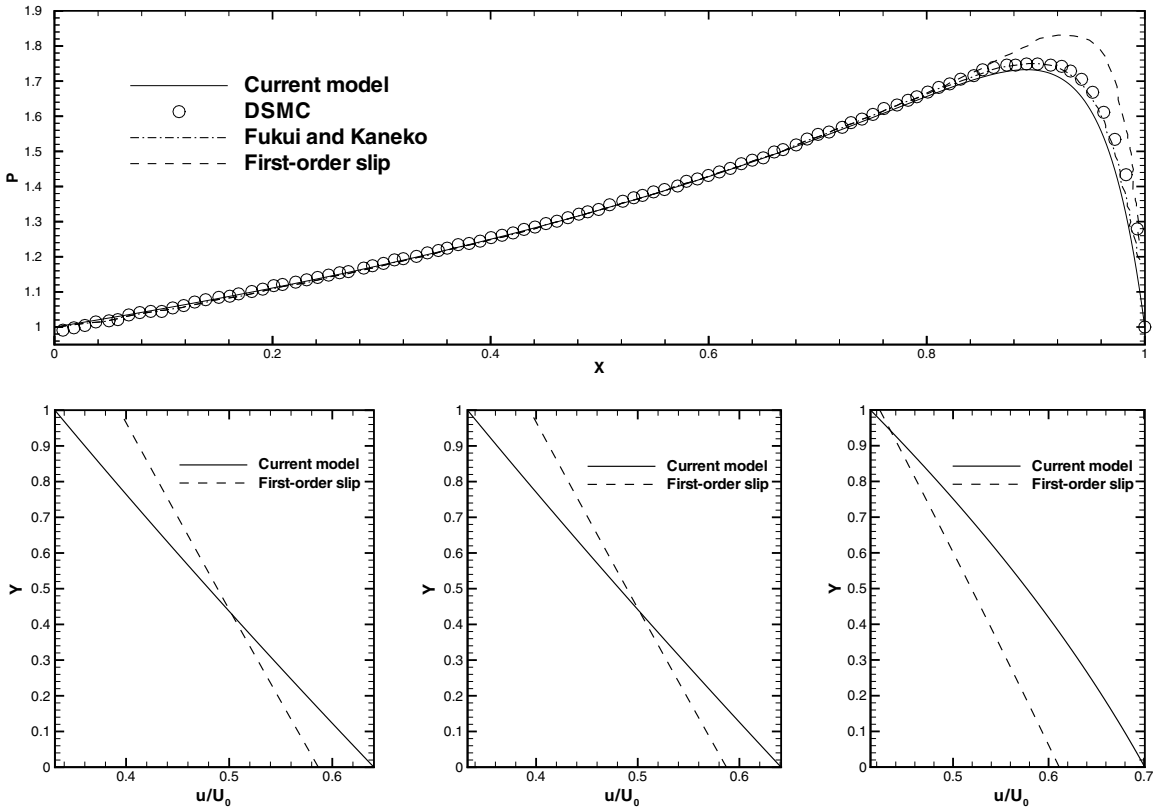

Figure 11. *Top*: pressure distribution for $Kn = 4.167$ and the bearing number $\Lambda = 1264$. *Bottom*: velocity distribution at various streamwise positions. Predictions based on the current and first-order slip models are shown. The cross-flow direction Y is normalized with the local bearing height $Y = y/h$.

The pressure drag forces are negligible in most slider-bearing configurations because of small angle of inclination of the floating slider. However, the effects of viscous shear stresses on the runner and slider surfaces are significant. The viscous shear stresses acting on the slider surface (τ_{xy}) allow the flexure in the slider suspension to rotate with very little resistance in the pitch and roll directions so that it can stay close to the recording surface despite undulations and asperities on the disk. The pitch and roll moments due to the viscous stresses are incorporated into the equations governing the dynamics of the slider-suspension assembly to accurately calculate pitch (ϕ) and roll (φ). The dynamic equations for ϕ and φ that require the shear stress contributions are given in [27]. However, the hydrodynamic definition of the shear stress requires modifications as the magnetic spacing reduces and rarefaction effects become important. In the absence of thermal-creep effects, the wall shear stress τ_{xy} can be explicitly expressed as the sum of the Couette and Poiseuille flow contributions.

The shear stress acting on the slider surface at any point is given by

$$\tau_{xy} = (\tau_{xy})_{\text{Couette}} + (\tau_{xy})_{\text{Poiseuille}}. \tag{26}$$

In section 2.1, we have formulated an empirical shear stress model for the plane Couette flows that is accurate in the entire Knudsen regime for $Ma < 0.3$. Rewriting equation (7) in dimensional form we get

$$(\tau_{xy})_{\text{Couette}} = -\frac{\mu_o U_o}{2h}\frac{aKn^2 + 2bKn}{aKn^2 + cKn + b}$$
$$a = 0.529690 \qquad b = 0.602985 \qquad c = 1.627666. \tag{27}$$

The plane Poiseuille flow shear stress is given by equation (14). Thus, the shear force acting on a differential area dA on the slider surface is given by

$$\mathrm{d}F_x = -((\tau_{xy})_{\text{Couette}} + (\tau_{xy})_{\text{Poiseuille}})\,\mathrm{d}A. \tag{28}$$

The total friction force can then be determined by integration over the bearing area. Using equations (27) and (13), we have

$$F_x = \int_0^L \left[\frac{\mu U_o}{2h}\left(\frac{aKn^2 + 2bKn}{aKn^2 + cKn + b}\right) + \frac{h}{2}\frac{\mathrm{d}p}{\mathrm{d}x}\right]\mathrm{d}x \tag{29}$$

where F_x is the total friction force per unit width acting on the slider surface. Also note that Kn is the local Knudsen number and is dependent on the local pressure. So, one should first convert Kn in equation (29) to the outlet Knudsen number Kn_o, using $Kn = Kn_o/(PH)$, before the integration.

Using equation (26) it is possible to calculate the pointwise distribution of shear stress on the runner and slider surfaces, for small or moderate angles of the slider inclination. While the shear stress on both the surfaces are typically equal for small angles of inclination, it is also important to emphasize the possibility of asymmetric shear stress distribution on the slider and runner surfaces when the angle of inclination is larger.

5. Conclusions

A self-consistent semi-analytical slip-based model, centered around the modified Reynolds equation is developed to accurately predict the *velocity and shear stress distribution,*

pressure profile and the *load capacity* in slider bearings for a wide range of Knudsen numbers ($Kn < 12$). We also presented a method to calculate the *skin friction and viscous drag* on the runner and slider surfaces separately. This is important to predict the pitch and roll moments in slider bearings. In addition, accurate prediction of viscous forces enables robust head-suspension design and calculation of actuator power consumption. Considering that other continuum-based slip models and the existing generalized lubrication models fail to predict the velocity distribution and skin friction in the transition and free molecular flow regimes, the new model delivers a level of physical information similar to that of exhaustive DSMC computations with minimal computational effort.

The new model is derived from the Navier–Stokes equations with the generalized slip models. However, it requires empirical corrections to the pressure-driven flow portion of the lubrication equation in the transition and free molecular flow regimes. We established this 'closure' using the Poiseuille flowrate database obtained from the two-dimensional Boltzmann equation solution. Due to this empirical closure, our model closely mimics the Fukui and Kaneko generalized lubrication model, derived using the *two-dimensional* Boltzmann equation. Hence, our model is not a mere semi-analytical/empirical substitute to the Fukui and Kaneko model, which is the current industry standard for air bearing design. We must admit that both our model and the Fukui and Kaneko model become invalid in the free molecular flow regime. This is due to the use of *two-dimensional* Boltzmann equation solution that results in an *unphysical* logarithmic increase in the Poiseuille flowrate as $Kn \to \infty$. Thus caution must be exercised while using both models for ultra-thin lubrication films. Despite this limitation, the new empirical model can be *calibrated* to match any other Poiseuille flow database, as demonstrated earlier in [14]. Empirical correction factors in the current model are valid for the classical slider-bearing geometry, and they hold as long as the Reynolds approximation is not violated.

Finally, the next generation ultra-high density storage units require magnetic spacings as low as 10 nm. Roughly 15 Å of this spacing comes from slider head overcoat thickness, 25 Å from the head thickness and 60 Å from the flying height [28]. In such small spacings, the surface/molecular force fields become significant within the thin film gap. Thus, we note that a free molecular flow analogy of nanoflows to low pressure rarefied gas flow will break down. Although advances in nanotechnology with regards to fabrication, characterization and tribology can result in slider bearings with nanoscale spacings, a fundamental understanding of the physics of thermal/fluidic transport in these length scales is still lacking.

References

[1] Karniadakis G E and Beskok A 2002 *Micro Flows: Fundamentals and Simulation* (New York: Springer)

[2] Gross W A, Matsch L A, Castelli V, Eshel A, Vohr J H and Wildmann M 1980 *Fluid Film Lubrication* (New York: Wiley)

[3] Burgdorfer A 1959 The influence of the molecular mean free path on the performance of hydrodynamic gas lubricated bearings *J. Basic Eng. Trans.* **81** 94–9

[4] Hsia Y and Domoto G 1983 An experimental investigation of molecular rarefaction effects in gas-lubricated bearings at ultra low clearances *J. Lubr. Technol.* **105** 120–30

[5] Gans R F 1983 Lubrication theory at arbitrary Knudsen number *J. Tribol.* **107** 431–33

[6] Fukui S and Kaneko R 1988 Analysis of ultra-thin gas film lubrication based on linearized Boltzmann equation. First report—derivation of a generalized lubrication equation including thermal creep flow *J. Tribol.* **110** 253–62

[7] Alexander F J, Garcia A J and Alder B J 1994 Direct simulation Monte Carlo for thin-film bearings *Phys. Fluids* **6** 3854–60

[8] Huang W and Bogy D B 1997 Three-dimensional direct simulation Monte Carlo method for slider air bearings *Phys. Fluids* **9** 1764–9

[9] Liu N and Ng E Y K 2001 The posture effects of a slider air bearing on its performance with a direct simulation Monte Carlo method *J. Micromech. Microeng.* **11** 463–73

[10] Mitsuya Y 1993 Modified Reynolds equation for ultra-thin gas lubrication using 1.5-order slip-flow model and considering surface accommodation coefficient *JSME Int. J.* **115** 289–93

[11] Hwang C C, Fung R F, Yang R F, Weng C I and Li W L 1996 A new modified Reynolds equation for ultra-thin film gas lubrication *IEEE Trans. Magn.* **32** 344–7

[12] Ng E Y K and Liu N 2002 Stress-density ratio slip-corrected Reynolds equation for ultra-thin gas bearing lubrication *Phys. Fluids* **14** 1450–7

[13] Bahukudumbi P, Park J H and Beskok A 2003 A unified engineering model for steady and quasi-steady shear driven gas microflows *J. Microscale Thermophys. Eng.* at press

[14] Beskok A and Karniadakis G E 1999 A model for flows in channels, pipes and ducts at micro- and nano-scales *J. Microscale Thermophys. Eng.* **3** 43–77

[15] Maxwell J C 1879 *Phil. Trans. R. Soc.* **170** 231–56

[16] Ohwada T, Sone Y and Aoki K 1989 Numerical analysis of the shear and thermal creep flows of a rarefied gas over a plane wall on the basis of the linearized Boltzmann equation for hard sphere molecules *Phys. Fluids* **1** 1588–99

[17] Kogan M 1969 *Rarefied Gas Dynamics* (New York: Plenum)

[18] Cercignani C and Daneri A 1963 Flow of a rarefied gas between two parallel plates *J. Appl. Phys.* **43** 3509–13

[19] Huang A, Giddens D and Bagnal C 1966 Rarefied gas flow between parallel plates based on the discrete ordinate method *Phys. Fluids* **10** 498–502

[20] Ohwada T, Sone Y and Aoki K 1989 Numerical analysis of the Poiseuille and thermal transpiration flows between two parallel plates on the basis of the Boltzmann equation for hard sphere molecules *Phys. Fluids* **1** 2042–9

[21] Aoki K 1989 Numerical analysis of rarefield gas flows by finite-difference method *Rarefield Gas Dynamics: Theoretical and Computational Techniques* E P Muntz, D P Weaves and D H Campbell (ed) pp 297–322

[22] Fukui S and Kaneko R 1990 A database for interpolation of Poiseuille flow rates for high Knudsen number lubrication problems *J. Tribol.* **112** 78–83

[23] Gaede W 1913 Die äubere reibung der gase *Ann. Phys., Lpz.* **41** 289

[24] Tison S 1993 Experimental data and theoretical modeling of gas flows through metal capillary leaks *Vacuum* **44** 1171–5

[25] Cercignani C 1963 Plane Poiseuille flow and Knudsen minimum effect *Proc. 3rd International Symposium on Rarefied Gas Dynamics* vol 1 ed J A Laurmann (New York: Academic) p 92–101

[26] Loyalka S and Hamoodi S 1990 Poiseuille flow of a rarefied gas in a cylindrical tube: solution of linearized Boltzmann equation *Phys. Fluids* A **2** 2061–5

[27] Crone R M, Kang S C and Jhon M S 1999 A new molecular gas lubrication theory suitable for head-disk interface modeling *J. Appl. Phys.* **85** 5594–6

[28] Menon A K 2000 Interface tribology for 100 Gb in^{-2} *Tribol. Int.* **33** 299–308